



**HAL**  
open science

## **Arabidopsis SMO2 modulates ribosome biogenesis by maintaining the RID2 abundance during organ growth**

Zhengfei Guo, Xiaoyu Wang, Yan Li, Aiming Xing, Chengyun Wu, Daojun Li, Chunfei Wang, Anne de Bures, Yonghong Zhang, Siyi Guo, et al.

### ► To cite this version:

Zhengfei Guo, Xiaoyu Wang, Yan Li, Aiming Xing, Chengyun Wu, et al.. Arabidopsis SMO2 modulates ribosome biogenesis by maintaining the RID2 abundance during organ growth. The Plant Journal, 2023, 114 (1), pp.96 - 109. 10.1111/tpj.16121 . hal-04116674

**HAL Id: hal-04116674**

**<https://univ-perp.hal.science/hal-04116674v1>**

Submitted on 5 Jun 2023

**HAL** is a multi-disciplinary open access archive for the deposit and dissemination of scientific research documents, whether they are published or not. The documents may come from teaching and research institutions in France or abroad, or from public or private research centers.

L'archive ouverte pluridisciplinaire **HAL**, est destinée au dépôt et à la diffusion de documents scientifiques de niveau recherche, publiés ou non, émanant des établissements d'enseignement et de recherche français ou étrangers, des laboratoires publics ou privés.

---

**Arabidopsis SMO2 modulates ribosome biogenesis by maintaining the RID2 abundance during organ growth**

Zhengfei Guo<sup>a,b,#</sup>, Xiaoyu Wang<sup>b,#</sup>, Yan Li<sup>a,b,#</sup>, Aiming Xing<sup>a,b,#</sup>, Chengyun Wu<sup>b,c</sup>, Daojun Li<sup>b</sup>, Chunfei Wang<sup>b</sup>, Anne de Bures<sup>d,e</sup>, Yonghong Zhang<sup>f</sup>, Siyi Guo<sup>b,c</sup>, Julio Sáez-Vasquez<sup>d,e</sup>, and Zhenguo Shen<sup>a</sup>, Zhubing Hu<sup>b,c</sup>

<sup>a</sup> College of Life Sciences, Nanjing Agricultural University, Nanjing 210095, China

<sup>b</sup> State Key Laboratory of Crop Stress Adaptation and Improvement, School of Life Sciences, College of Agriculture, Henan University, Kaifeng 475004, China

<sup>c</sup> Sanya Institute of Henan University, Sanya, Hainan 572025, China

<sup>d</sup> Centre National de la Recherche Scientifique, Laboratoire Génome et Développement des Plantes, Unité Mixte de Recherche 5096, 66860, Perpignan, France

<sup>e</sup> Université Perpignan Via Domitia, Laboratoire Génome et Développement des Plantes, Unité Mixte de Recherche 5096, 66860, Perpignan, France

<sup>f</sup> Laboratory of Medicinal Plant, Hubei Key Laboratory of Wudang Local Chinese Medicine Research, Academy of Bio-Medicine Research, School of Basic Medicine, Hubei University of Medicine, Shiyan 442000, China

ORCID IDs: 0000-0002-5394-9864 (Z.H.); 000-0002-2717-7995 (J.S.)

**Running title:** SMO2 Participates in Ribosome Biogenesis

# These authors contributed equally to this work

**Corresponding author:**

Zhenguo Shen

College of Life Sciences

Nanjing Agricultural University, Nanjing 210095, China

zgshen@njau.edu.cn

This article has been accepted for publication and undergone full peer review but has not been through the copyediting, typesetting, pagination and proofreading process which may lead to differences between this version and the [Version of Record](#). Please cite this article as doi: [10.1111/tpj.16121](https://doi.org/10.1111/tpj.16121)

This article is protected by copyright. All rights reserved.

Zhubing Hu

State Key Laboratory of Crop Stress Adaptation and Improvement

School of Life Sciences

Henan University, Kaifeng 475004, China

E-mail: zhubinghu@henu.edu.cn

**One-sentence summary:** SMO2 maintains the abundance of the methyltransferase RID2 to participate in ribosomal RNA processing and repress nucleolar stress.

### Footnotes

<sup>1</sup>Address correspondence to zgshen@njau.edu.cn and zhubinghu@henu.edu.cn

The author responsible for distribution of materials integral to the findings presented in this article in accordance with the policy described in the Instructions for Authors is:

Zhubing Hu (zhubinghu@henu.edu.cn).

## ABSTRACT

Ribosome biogenesis is a process of making ribosomes that is tightly linked with plant growth and development. Here, through a suppressor screen for the *smo2* mutant, we found that lack of a ribosomal stress response mediator, ANAC082 partially restored growth defects of the *smo2* mutant, indicating SMO2 is required for the repression of nucleolar stress. Consistently, the *smo2* knock-out mutant exhibited typical phenotypes characteristic of ribosome biogenesis mutants, such as pointed leaves, aberrant leaf venation, disrupted nucleolar structure, abnormal distribution of rRNA precursors and enhanced tolerance to aminoglycoside antibiotics that target ribosomes. SMO2 interacted with ROOT INITIATION DEFECTIVE 2 (RID2), a methyltransferase-like protein required for pre-rRNA processing. SMO2 enhanced RID2 solubility in *E. coli* and the loss of function of *SMO2* in plant cells reduced RID2 abundance, which may result in abnormal accumulation of FIBRILLARIN 1 (FIB1) and NOP56, two key nucleolar proteins, in high-molecular-weight protein complex. Taken together, our results characterized a novel plant ribosome biogenesis factor, SMO2 that maintains the abundance of RID2, thereby sustaining ribosome biogenesis during plant organ growth.

**Keywords:** SMO2, Pre-RNA processing, Ribosome biogenesis, Nucleolar stress, RID2, ANAC082

## INTRODUCTION

Ribosomes are the molecular machines responsible for protein synthesis, and their function is evolutionarily conserved across all kingdoms of life. In plant cells, the cytoplasmic (80S) ribosome is made up of two subunits, a 60S large subunit (LSU) and a 40S small subunit (SSU) (Sáez-Vásquez and Delseny, 2019). The 60S LSU is composed of three ribosomal RNAs (rRNAs) (25S, 5.8S, and 5S) and ~40 ribosome protein large subunits (RPLs), and the 40S SSU contains an 18S rRNA and ~30 ribosome protein small subunits (RPSs). Ribosome biogenesis begins with the transcription of the 45S rDNA genes in the nucleolus to produce a single polycistronic precursor, 45S pre-rRNA (Weis et al., 2015). The resulting pre-rRNA transcript folds to associate with many ribosome biogenesis factors, an RNA chaperone and ribosomal proteins and is concurrently processed to generate a correctly assembled SSU Processome (Sáez-Vásquez and Delseny, 2019). Subsequently, the SSU Processome transitions to the pre-40S, which requires the release of most of biogenesis factors and the endonucleolytic cleavages of the pre-rRNA (Barandun et al., 2018; Du et al., 2020). In yeast and human cells, the assembly and disassembly of SSU Processome are tightly coordinated with the pre-rRNA processing and the assembly of the ribosomal precursor particles of 60S LSU and 40S SSU that are exported to the cytoplasm, where the final assembly of the 80S ribosome is completed (Du et al., 2020; Singh et al., 2021; Vanden Broeck et al., 2022). However, these processes remain largely unknown in plants.

In view of the central function of ribosomes as cellular protein producers, ribosome biogenesis is tightly linked to development and stress responses in all species. For example, aberrant ribosome biogenesis is typically associated with diverse developmental diseases known as ribosomopathies in humans (Narla and Ebert, 2010; Farley-Barnes et al., 2019). Similarly, many plant mutants with defects in ribosome biogenesis are known to be embryonic lethality or to have pleiotropic developmental abnormalities, such as retarded growth and narrow and pointed leaves (Wu et al., 2021). These defects seem to be associated with structural disorders of the nucleolus resulting in cell cycle arrest and senescence (cell death/apoptosis), which are commonly referred to as nucleolar stresses (Ohbayashi et al., 2017; Matos-Perdomo and Machín, 2019).

Under nucleolar stress, mammalian cells activate the Murine Double Minute2 (MDM2)/tumor protein53 (p53) pathway to coordinate cellular responses (Liu et al., 2016). However, plants lack homologs of either p53 or MDM2 (Hu et al., 2016; Sáez-Vásquez and Delseny, 2019). Recently, a NAC-family transcription factor, ANAC082, was characterized as a potential ribosomal stress response mediator because its loss of function could alleviate the developmental defects in several ribosomal mutants (Ohbayashi et al., 2017; Wang et al., 2020), suggesting that plants may also have a pathway involved in responses to nucleolar stress.

The Arabidopsis mutant *small organ 2 (smo2)* shows dramatic reduction in the sizes of organs including the root, stem, leaves, flowers, and fruits (Hu et al., 2010). *SMO2* encodes an Arabidopsis tRNA methyltransferase 112 (TRM112) homolog that participates in the modulation of cell cycle progression, and the Arabidopsis *smo2* mutant exhibits decreased cell proliferation (Hu et al., 2010). In this study, we found that *SMO2* interacts with ROOT INITIATION DEFECTIVE 2 (RID2), a methyltransferase-like protein involved in pre-rRNA processing. Deficiency of *SMO2* reduced RID2 abundance and led to the disruption of ribosome biogenesis. Collectively, our results demonstrated that *SMO2* acts as a cofactor to maintain the abundance of RID2, thereby preventing the activation of nucleolar stresses that inhibit plant growth.

## RESULTS

### **Growth retardation in the *smo2* mutant was partially suppressed by ANAC082 deficiency.**

Previously, we reported that *SMO2* modulates cell proliferation during organ growth, with loss of function leading to a drastically short root, among other mutant traits (Hu et al., 2010). To investigate the underlying mechanism, we mutagenized *smo2* seeds with ethyl-methanesulfonate to screen for suppressors of growth defects using root length as an indicator. In total, 123 suppressors of *smo2* (designated as *ssm*) were obtained. Subsequently, these 123 *ssm* mutants were backcrossed with the *smo2* mutant to generate F1 progenies and F2 population by F1 self-pollination. F2 plants that showed longer roots than the *smo2* mutants made a mixed DNA pool and employed a

next-generation sequencing-based strategy to characterize the casual mutation. Nine alleles of *ANAC082* were isolated and had a longer root than its parental line, the *smo2* mutant (Figure 1A and 1B; Supplemental Figure 1). A mutant, *ssm1-8 smo2* was randomly selected for further analysis. The *ssm1-8 smo2* mutant has a causal mutation in the *SSM* locus that was pinpointed to the codon at position 433 of the *AT5G09330* gene, in which there was a substitution from glutamine (CAG) to a premature stop codon (TAG). Furthermore, an *anac082-4* T-DNA insert mutation was crossed into the *smo2* mutant to generate the *anac082-4 smo2* double mutant and examined primary root growth. Unsurprisingly, primary root growth of *anac082-4 smo2* was restored to an extent similar to that of *ssm1-8 smo2* (Figure 1B and 1D; Supplemental Figure 2A and 2C). Additionally, we crossed *ssm1-8 smo2* with *anac082-4 smo2* to produce F1 progenies and found all F1 progenies exhibited longer roots than the *smo2* mutant, confirming that ANAC082 is involved in the growth inhibition by the *smo2* mutation. Beside the partial suppression of primary root growth, we noticed that the rosette defects in the *smo2* mutant were significantly less severe in the absence of ANAC082 (Figure 1C and 1E; Supplemental Figure 2B). These observations support the presence of a genetic link between SMO2 and ANAC082 in the regulation of root (organ) growth.

### The *smo2* mutant shows nucleolar stress

ANAC082 has been shown to participate in the response to nucleolar stress during plant growth (Ohbayashi et al., 2017). The mutations on *ANAC082* alleviate the growth defects of the *smo2* mutation, hinting that the *smo2* mutant may show nucleolar stress. To test this speculation, we first crossed a nucleolar-specific green fluorescent protein (GFP) marker, FIB1-GFP, into *smo2* to observe the nucleolus size. The *smo2* mutant had obviously larger nucleoli than Col-0 (Figure 2A). Furthermore, we performed immunoblotting analysis with FIB1 antibody to measure area ratio of nucleolus/nucleus and found that the *smo2* mutant exhibited higher area ratio of nucleolus/nucleus compared to Col-0 (Figure 2B), further indicating the role of SMO2 repressing nucleolar stress. This enhanced ratio in the *smo2* mutant could be also partially

suppressed by the loss of function of *ANAC082*; while no difference in area ratio of nucleolus/nucleus was detected between *anac082-4* and Col-0 (Figure 2B).

It is worth noting that the *smo2* mutant exhibits other pleiotropic developmental defects, namely pointed rosette leaves, aberrant leaf venation accompanied by disconnected free ends, unfertilized ovules, and a decreased number of normal seeds in the silique (Figure 3). These defects were apparently restored in the *smo2* complementation line (*C-smo2*) (Figure 3), which harbors a 2.5-kb wild-type *SMO2* genomic DNA fragment from the promoter to the 3' -untranslated region (Hu et al., 2010). These developmental defects resemble those of several known ribosome biogenesis mutants (Hang et al., 2014; Sáez-Vásquez and Delseny, 2019), implying that *SMO2* may play a role in ribosome biogenesis.

### **Deficiency of *SMO2* leads to defective rRNA processing**

Ribosome biogenesis initiates in the nucleolus (Sáez-Vásquez and Delseny, 2019). rRNA molecules are structural components of the ribosome (Weis et al., 2015). Aberrant processing of pre-rRNA is usually associated with nucleolus disorganization and leads to nucleolar stress (Hang et al., 2021). To test whether the deficiency of *SMO2* results in defective pre-rRNA processing, we performed northern blot analyses to determine the abundance of pre-rRNA intermediates using two specific probes (S7 and S43) against internal transcribed spacer 1 (ITS1) and a specific probe (S9) against ITS2, (Figure 4A). As shown in Figure 4B, the intermediates 32S, 27SA/B, and 18S-A3 accumulated at higher levels in the *smo2* mutant than in the wild-type plants (Col-0) and the complementation line (*C-smo2*). These results demonstrate that *SMO2* is involved in pre-rRNA processing.

Next, we performed a set of circular reverse transcription polymerase chain reaction (cRT-PCR) assays to detect the precise 3' and 5' ends of pre-rRNA intermediates. In Arabidopsis, up to three 35S pre-rRNA processing pathways have been proposed, namely the minor 5'ETS-first pathway, the major ITS1-first pathway and the ITS2-first pathway (Sáez-Vásquez and Delseny, 2019). Before the A2 cleavage, 32S pre-rRNA is produced by the 5'ETS-first pathway, and 18S-A3 and 27SA/27SB

pre-rRNAs are mainly produced by the major ITS1-first pathway. The 32S rRNA intermediates were notably accumulated in the *smo2* mutant compared with Col-0 (Figure 5A, 5B and 5E). We also found that two pre-18S rRNA intermediates, P-A3 and P'-A3, were obviously less abundant in the *smo2* mutant, whereas 18S-A3 was more abundant (Figure 5C-F). P-A3, P'-A3, and 18S-A3 are produced by the major pre-rRNA processing pathway ITS1-first, demonstrating that SMO2 mainly functions in this pathway. However, accumulation of 32S indicates that the minor processing pathway 5'ETS-first is also affected.

### **SMO2 interacts with RID2**

SMO2 is an Arabidopsis homolog of mammalian TRM112 (Hu et al., 2010). It has been shown that the yeast TRM112 counterpart interacts with BUD23 to participate in 18S rRNA processing (Figaro et al., 2012; Sardana and Johnson, 2012). It is interesting to note that RID2, the yeast BUD23 homolog in Arabidopsis, has also been found to be involved in pre-rRNA processing (Ohbayashi et al., 2011), and the *rid2-1* mutant has the same defects we observed in the *smo2* mutant (Ohbayashi et al., 2011). We therefore postulated that the molecular role of SMO2 in plant pre-rRNA processing may be achieved by the regulation of RID2 activity. To test this, we first performed bimolecular fluorescence complementation (BiFC) analysis in *Nicotiana benthamiana* leaves. After transient co-expression of RID2-YFP<sup>N</sup> (N-terminal half of yellow fluorescent protein) and SMO2-YFP<sup>C</sup> (C-terminal half of YFP), YFP fluorescence was observed, but no YFP fluorescence was detected in leaves co-expressing either YFP<sup>C</sup> and RID2-YFP<sup>N</sup> or SMO2-YFP<sup>C</sup> and YFP<sup>N</sup> (Supplemental Figure 3A). This YFP signal was located within the nucleus labeled with the mCherry protein fused with a nuclear localization signal (NLS-mCh) (Supplemental Figure 3B) and overlapped with the nucleolus marker FIB1-mRFP (Figure 6A), suggesting that the interaction of SMO2-RID2 occurs in the nucleolus.

To provide further evidence for SMO2-RID2 interaction, we performed a pull-down assay in which SMO2 was co-expressed with either a polyhistidine and small ubiquitin-related modifier protein (SUMO)-tagged RID2 (RID2-SUMO-6xHIS) or the

control SUMO-6xHIS protein in *Escherichia coli*, followed by purification on Nickel-NTA agarose resin. RID2-SUMO-6xHIS, SUMO-6xHIS, and SMO2 were detected in the flow through using His ( $\alpha$ -His) and/or SMO2 ( $\alpha$ -SMO2) antibodies (Figure 6B). During the purification step, SMO2 co-eluted with RID2-SUMO-6xHIS but not SUMO-6xHIS (Figure 6B), suggesting that SMO2 interacts with RID2 *in vitro*. The SMO2-RID2 interaction was further validated *in vivo* by performing co-immunoprecipitation assay using plant cells (Figure 6C).

### **SMO2 regulates RID2 abundance**

Strikingly, we noticed that most of the RID2-SUMO-6xHIS protein was present in *E. coli* inclusion bodies and was insoluble, whereas the solubility of RID2-SUMO-6xHIS was increased when it was co-expressed with SMO2 (Figure 7A), providing an *in vitro* clue that SMO2 might be essential for RID2 solubility as well as maintenance of its functional structure. To investigate the reciprocal impacts of these proteins *in vivo*, we generated a reliable RID2-GFP overexpression line and crossed it with the *smo2* mutant. Compared with the strong intensity of RID2-GFP fluorescence in wild type, only faint fluorescence could be observed in the *smo2* mutant, suggesting that SMO2 is indispensable for RID2 abundance in plants (Figure 7B and 7C). To provide more convincing evidence, we generated an anti-Arabidopsis RID2 antibody ( $\alpha$ -RID2) by immunizing rabbits and then detected the RID2 protein levels in Col-0 and the *smo2* mutant. Consistent with the role of SMO2 in maintaining RID2 abundance, a significant decrease of RID2 in the *smo2* mutant was observed (Figure 7D). Meanwhile, we examined the RID2 transcripts and found that RID2 transcript level in the *smo2* mutant is significantly higher than that in Col-0 (Supplemental Figure 4). These data explicitly demonstrate that SMO2 is crucial for RID2 abundance.

### **The *smo2* mutant is tolerant to antibiotics**

rRNAs are the linchpins of ribosome biogenesis (Sáez-Vásquez and Delseny, 2019). In this regard, the defects of the *smo2* mutant in pre-rRNA processing prompted us to investigate the roles of SMO2 in ribosome function by monitoring plant responses

to various antibiotics. We found that the *smo2* mutant displays remarkable resistance to three aminoglycoside antibiotics, namely gentamicin, spectinomycin, and kanamycin, and retains a higher total chlorophyll content in its cotyledons compared with the wild type (Supplemental Figure 5). Aminoglycoside antibiotics preferentially target the ribosomal acceptor site (A site) during translation and lead to a delay in translocation and translation elongation by altering allosteric control, disrupting the decoding progress, and causing misreading (Kanazawa et al., 2018), indicating that the *smo2* mutation might lead to the change of ribosome structure.

### **FIB1 and NOP56 were accumulated in high-molecular-weight protein complex in the *smo2* mutant**

The yeast RID2 homolog acts to dissociate assembly factors at the transition of the ribosomal small subunit (SSU) Processome towards a pre-40S particle (Black et al., 2020). Because SMO2 affects RID2 abundance (Figure 8), we speculated that SMO2 deficiency disrupts the disassembly of the SSU Processome. To address this, we examined the levels of two key nucleolar components, FIB1 and NOP56, which were previously used to indicate defective disassembly of SSU Processome in the *prmt3* mutant (Hang et al., 2021). We observed dramatic accumulation of FIB1 and NOP56 in the *smo2* mutant (Supplemental Figure 6). Furthermore, gel filtration analysis showed that high molecular weight fractions of FIB1 and NOP56 in the *smo2* mutant accumulated in higher levels than Col-0 and *C-smo2* plants, suggesting that SMO2 promotes the disassembly of the 90S/SSU Processome at early pre-rRNA processing stages (Figure 8).

### **DISCUSSION**

Previously, we reported that SMO2 modulates cell cycle progression during organ growth in Arabidopsis (Hu et al., 2010); however, its underlying mechanism is largely elusive. Here, we found that SMO2 is required for proper ribosome biogenesis, a crucial biological event for plant growth and development. In support of this finding, the *smo2* mutant exhibited defects reminiscent of ribosomal mutants, such as serrated and pointed

leaves, partial infertility, and aberrant venation in the cotyledons and true leaves (Figure 3). Furthermore, the mutant exhibited abnormal nucleolus morphology (Figure 2), aberrant accumulation of pre-rRNA intermediates (Figure 4 and 5), and increased tolerance to aminoglycoside antibiotics (Supplemental Figure 5).

The depletion of SMO2 may activate nucleolar stress, which, at least partially, contributes to the aberrant organ growth in the *smo2* mutant (Figure 1) (Hu et al., 2010). The transcriptional factor p53, which is thought to drive animal cell cycle arrest or apoptosis in response to nucleolar stress, is not present in plants. However, the plant functional counterpart of p53 specifically in sensing of nucleolar stress, a NAC-family transcription factor, ANAC082, has been identified to coordinate plant growth and development in response to nucleolar stress (Ohbayashi et al., 2017); the loss of *ANAC082* alleviates the developmental defects in several ribosomal mutants (Ohbayashi et al., 2017; Wang et al., 2020). In our study, the *smo2 anac082* double mutant displayed better growth fitness in comparison with the *smo2* single mutant (Figure 1B-1E; Supplemental Figure 2), implying that *smo2* deficiency causes nucleolar stress. It is expected that there are downstream effectors of ANAC082 involved in cell division regulation that cope with *smo2*-induced nucleolar stress, which remain to be identified in the future.

In addition, in a previous study, we showed that the *smo2* mutant shows increasing expression of the G2/M marker CYCB1;1 $\beta$ -glucuronidase during organogenesis, suggesting that the mutant experiences an arrest in the G2 or M phase during cell cycle progression (Hu et al., 2010). The same type of arrest has been widely reported for cell cycle-related mutants suffering from DNA damage (Hu et al., 2016; Schnittger and De Veylder, 2018), providing a clue that SMO2 interferes with cell cycle progression by regulating cell division effectors identical to those involved in DNA damage responses. For example, SIAMESE-RELATED cyclin-dependent kinase inhibitors, such as SMR5 and SMR7, are directly regulated by a plant functional p53 homolog, a suppressor of gamma response 1 (SOG1) (Yi et al., 2014; Yoshiyama, 2016). The involvement of these known effectors makes them good candidates for studies aimed at deeper dissection of SMO2 functions.

In the *smo2* mutant, obvious accumulation of 32S rRNA and 27SA/27SB pre-rRNAs was observed (Figure 4 and 5), indicating that the defective cleavage in the *smo2* mutant occurs around the A2 site (Figure 9). As the A2 site is cleaved by the disassembly of the SSU Processome in eukaryotic organisms (Black et al., 2020), we postulate that SMO2 is required for the disassembly of the SSU Processome at the transition of the SSU Processome to pre-40S particles. To a great extent, SMO2 serves the same function as TRM112 does in yeast (Black et al., 2020). In agreement with this, the yeast mutant  $\Delta trm112$  also shows defects in pre-rRNA processing and cell growth. Different from the Arabidopsis *smo2* mutant, TRM112-deficient yeast exhibits over-accumulation of 35S pre-rRNA, but a significant reduction of precursors of the 5.8S and 25S rRNAs (the 7S and 27S pre-rRNAs) (Figaro et al., 2012; Sardana and Johnson, 2012). In TRM112-knock-down human cells, the level of the 18S-A3 precursor was also increased, but 30S was moderately reduced (Zorbas et al., 2015). These different accumulation patterns of pre-rRNA precursors among various SMO2/TRM112-deficient organisms may be consistent with different rRNA processing pathways existing in different organisms (Sáez-Vásquez and Delseny, 2019).

In yeast, TRM112 acts as cofactor of BUD23 methyltransferases and is required for Bud23 stability to regulate BUD23 abundance (Black et al., 2020). In this study, we found that SMO2 interacts with RID2, an Arabidopsis homolog of BUD23, demonstrating that the TRM112-BUD23/SMO2-RID2 complex is widely present in eukaryotic organisms. In the SMO2-depleted plants, a dramatic reduction in RID2 abundance was detected compared with the wild-type plants (Figure 7). A weak *RID2* mutant, *rid2-1*, displays similar defects as the *smo2* mutant including defects in organ growth and pre-rRNA processing (Ohbayashi et al., 2011), suggesting that the role of SMO2 in pre-rRNA processing may be achieved by maintaining the availability of RID2. Yeast RID2 homolog, BUD23 promotes the final disassembly of the small subunit Processome (Black et al., 2020). In this study, we also observed an enrichment of NOP56 and FIB1 in high-molecular-weight protein complex in the *smo2* mutant, suggesting that SMO2-RID2 complex is functional conserved in the disassembly of the small subunit Processome between plant and yeast. Furthermore, this abnormal

accumulation might increase the activity of 90S/SSU Processome, because the processing of P-A3 and P'-A3 pre-rRNAs in the *smo2* mutant was increased, which result in reduction of their levels (Figure 5).

Besides Bud23, TRM112 interacts with several other methyltransferases, which are involved in the methylation of tRNA, rRNA, and protein in yeast and/or human cells. TRM112 forms a complex with two tRNA methyltransferases, TRM11 and TRM9. Similar to yeast TRM9 and TRM11 (Purushothaman et al., 2005), Arabidopsis TRM9 and TRM11 are required for the U34 modifications 5-methoxycarbonylmethyluridine and the methylation of methyl-2-guanosine at position 10, respectively (Chen et al., 2010; Leihne et al., 2011). The growth of Arabidopsis TRM9 loss-of-function mutant is indistinguishable from that of wild-type plant (Leihne et al., 2011), while the Arabidopsis TRM11 mutant exhibits early flowering and a short root (Chen et al., 2010). TRM112 is also reported to act as a cofactor of the human 18S rRNA m6A methyltransferase METTL5 and the methyltransferase of the eukaryotic release factor 1, HEMK2 (Heurgué-Hamard et al., 2006; Li et al., 2019; Van Tran et al., 2019). There are METTL5 and HEMK2 homologs in Arabidopsis according to genome annotations, even though METTL5 has not been characterized in plants. Recently, Arabidopsis HEMK2 was reported to participate in the termination of translation, and lack of HEMK2 was found to cause severe developmental defects (Kailasam et al., 2020). Considering the growth defects in the Arabidopsis loss-of-function mutants *hemk2* and *trm11* (Chen et al., 2010; Kailasam et al., 2020), it is mostly likely that SMO2 acts as a cofactor of Arabidopsis HEMK2 and TRM11 and regulates their stability to fine-tune organ growth. In addition, SMO2 modulates abscisic acid responses during seed germination (Hu et al., 2010). Therefore, it will be interesting to investigate how SMO2 coordinates distinct biological processes (ribosome disassembly, translation release, tRNA methylation, and rRNA modification) in response to developmental and environmental cues in plants.

Taken together, we propose a working model to illustrate how SMO2 modulates ribosomal biogenesis during plant growth and development (Supplemental Figure 8). In wild-type plants, SMO2 ensures that the SSU Processome is properly disassembled

into pre-40S particle, thereby sustaining protein translation for organ growth and alleviating nucleolar stress. In the *smo2* mutants, however, the loss of SMO2 reduces RID2 abundance, leading to defects in disassembly of the SSU Processome and pre-rRNA processing. These defects in turn trigger nucleolar stress and protein translation errors. In response to nucleolar stress, ANAC082-dependent stress responses are activated to delay cell cycle progression. The partial recovery of organ growth in *anac082-4 smo2* may be due to abnormal protein translation.

## METHODS

### Plant Materials and Growth Conditions

*Arabidopsis thaliana* seeds were surface sterilized and plated on half-strength Murashige & Skoog (MS) medium supplemented various sugars and antibiotics as indicated. After 2 days at 4°C, the seeds were transferred into a plant incubator (22°C and a 16/8-hour day/night photoperiod) for further germination and growth. The *smo2* mutant, *smo2* complementation line (*C-smo2*), and *anac082-4* mutant (SALK\_132606) were described previously (Hu et al., 2010; Ohbayashi et al., 2017).

### Screen of the Suppressors of the *smo2* Mutants and the Isolation of Causal Mutation

Around 2.5 g *smo2* seeds (M0 generation) were soaked in a 50 mL plastic tube with 40 mL of 100 mM phosphate buffer at 4°C overnight. The tube was put upright to allow the seeds to settle and decant the excess phosphate buffer. Next, 40 mL of fresh 100 mM phosphate buffer containing a final concentration of 0.4% ethyl methanesulpho nate (EMS) were added into the tube and incubated 8 h at room temperature with gentle nutation. The EMS-mutagenized *smo2* seeds were washed thoroughly 20 times with water and planted on 1/2 MS medium and subsequently transferred into the soil. Approximately the seeds of 30,000 M1 plants were collected for 200 pools and each pool contained the seeds of 150 M1 plants. Approximately 3000 M2 seeds from each pool were screened using root length as an indicator to obtain the suppressors of the s*mo2* mutant (*ssm* mutant). Next, the suppressors were back-crossed with the *smo2*

mutant to generate F1 progenies and F2 population by F1 self-pollination. F2 plants with long roots to make a mixed DNA pool and employed a next-generation sequencing-based strategy to clone the casual mutation with the Mutmap tool (Takagi et al., 2015).

**Analysis of cotyledon and leaf venation patterns** The cotyledons and first leaves of 21-day-old plants were fixed overnight in a solution consisting of 90% (volume/volume) ethanol and 10% (volume/volume) acetic acid at room temperature. Next, the samples were dehydrated in an ethanol series and cleared overnight with an HCG solution (chloral hydrate: glycerol: water = 8:1:2, weight: volume: volume). The venation patterns were drawn from images photographed with an Olympus microscope.

### **Analysis of Nucleoli**

For the observatin of the nucleolus, the open reading frame of *FIB1* was cloned into the entry vector pDONR207 and then recombined into the vector pCambia1305-GFP via an LR reaction to generate the 35S:FIB1-GFP plasmid, which was transformed into wild-type plants to obtain FIB1-GFP transgenic plants (FIB1-GFP/Col-0). Subsequently, FIB1-GFP was introduced into the *smo2* mutant to generate FIB1-GFP/*smo2* plants. The resulting plants harboring FIB1-GFP were used to observe nucleolus morphology with confocal laser-scanning microscopy. The nuclei and nucleoli of Col-0, *smo2*, *anac082-4* and *anac082-4 smo2* were measured as described previously by immunolocalization (Pasternak et al., 2015). Simply, the roots of 7-d-old seedlings were sampled into 24-well microplates and fixed for 40 min at 37 °C with PIPES buffer solution (50 mM PIPES, pH 6.9, 2% paraformaldehyde, 5 mM MgSO<sub>4</sub>, and 5mM EGTA, pH 6.9 and 0.1% Triton X-100). A 1:500 dilution of primary FIB1 antibody and a 1:1000 dilution of the Alexa Fluor 488-labeled Goat Anti-Mouse IgG secondary antibody from Beyotime (A0423) were used. Nuclei were stained for 10 min with 0.5µg mL<sup>-1</sup> DAPI and washed for 5 min before mounting the samples on slides. The cell nucleolus and nuclei in root meristem zone were observed with confocal laser-scanning microscopy and the size was measured with Image J tools.

### Northern Blot Analysis, Circular RT-PCR Assay and Quantitative RT-PCR

Total RNA was isolated from 14-day-old seedlings using TRIzol reagent (Takara, Dalian, China) according to the manufacturer's instructions. To detect the accumulation of pre-rRNAs, northern blotting was performed as previously described (Hang et al., 2014). Total RNA (10 µg) was separated on a 1.2% (w/v) agarose/formaldehyde gel and transferred to a Hybond N+ membrane by capillary elution. The DNA probes were labeled with  $\gamma$ -<sup>32</sup>P-ATP by T4 polynucleotide kinase (New England Biolabs, M0201). Hybridization was performed overnight at 45 °C in Church buffer. The blots were washed and exposed to a storage phosphor screen. The signals were detected by a Typhoon TRIO scanner.

The 5' and 3' extremities of various rRNA precursors were determined by cRT-PCR. A total of 10 µg RNA was self-ligated using T4 RNA ligase. cDNAs were synthesized using the PrimeScript™ RT reagent Kit (Takara, Dalian, China) and amplified with gene-specific primers (Supplemental Table 1).

The *RID2* transcription expression was analyzed by quantitative RT-PCR with a LightCycler 480 (Roche). For each reaction, three technical repeats and three biological repeats were done. The relative expression of *RID2* was normalized by the two reference genes, *ACTIN2* and *EMB2386*. Primers of *RID2*, *ACTIN2* and *EMB2386* for RT-PCR are listed in Supplemental Table 1.

**Analysis of SMO2-RID2 interactions** For BiFC assays, **plasmids** were constructed using the 35S-Px-nYFP and 35S-Px-nCFP vectors. The open reading frames of *RID2* and *SMO2* were cloned into the entry vector pDONR207, and then recombined into the empty vectors via LR reactions to generate *RID2*-nYFP and *SMO2*-cYFP. These constructs were transformed into the *Agrobacterium* AH109 strain by heat shock transformation. *N. benthamiana* leaves were infiltrated with the mixed *Agrobacterium* strains. Fluorescence signals were detected 48 h after infiltration using a confocal laser-scanning microscope (FV10-ASW, Olympus, Tokyo, Japan) with excitation at 488 nm and detection with a 500–530 nm band-pass filter for YFP.

For co-elution assays, the open reading frames of *RID2* and *SMO2* without stop codons were amplified and digested by *Nde* I and *Bam*HI. The resulting fragments of *RID2* and *SMO2* were cloned into the vectors pSUMO-His6 and pET11a. Subsequently, the plasmids were transformed/co-transformed into *E. coli* strain BL21 (DE3). HIS-tagged *RID2* (*RID2*-SUMO-6HIS) and *SMO2* were induced by IPTG (0.3 mM) when the optical density of the bacteria at OD<sub>600</sub> nm was 0.6. After overnight growth, the cells were collected and lysed with buffer (20 mM Tris-HCl, 500 mM NaCl, 10 mM imidazole, 10% glycerol, 1% Triton-100, and 1:200 protease inhibitor cocktail). After centrifugation, the supernatant was loaded on Ni-NTA resin. The column was washed with elution buffer (20 mM Tris-HCl, 500 mM NaCl, 10% glycerol) with an imidazole gradient. The eluted fractions were collected. The proteins were separated by SDS-PAGE and stained with Coomassie blue or transferred to nitrocellulose for the detection of *RID2*-SUMO-6xHIS and SUMO-6xHIS with anti-His antibodies (GenScript, A00186) and *SMO2* with a specific antibody generated in our lab.

For the co-immunoprecipitation assay, the *RID2* antibody was captured by protein A/G magnetic beads. Total proteins from Col-0 and 35S:*SMO2*-Flag plants were extracted and incubated with the protein A/G magnetic beads and beads with *RID2* antibody. After washing, 5% of the total protein from Col-0 and 35S:*SMO2*-Flag plants and protein after Co-IP were separated by SDS-PAGE and transferred to nitrocellulose for the detection of *RID2* with a specific antibody and *SMO2* with Flag antibody (Merk, F7425).

### **Analysis of *RID2* Solubility**

For analyzing the solubility of *RID2* in *E. coli* cells, *RID2*-SUMO-6xHIS and *SMO2* were expressed in *E. coli* strain BL21 (DE3), either separately or together, with the plasmids mentioned above. The non-induced cells and cells induced with IPTG (0.3 mM) were collected and lysed with buffer (20 mM Tris-HCl, 500 mM NaCl, 10 mM imidazole, 10% glycerol, 1% Triton-100, and protease inhibitors). The pellets and soluble proteins were separated by centrifugation for the detection of *RID2* and *SMO2*.

For the analysis of *RID2* abundance in plants, we first generated 35S:*RID2*-GFP

transgenic plants (*RID2-GFP/Col-0*), which were then crossed with the *smo2* mutant to generate *35S:RID2-GFP* in the *smo2* background (*RID2-GFP/smo2*). Fluorescence signals were detected under a confocal microscope and quantified as an indicator of RID2 stability in plants. For the direct measurement of RID2 in plants, seedlings (0.2 g) were ground in lysis buffer (50 mM Tris-HCl [pH 8.0] 10 mM EDTA, 1% SDS, 1 mM DTT, and protease inhibitors). The protein levels were detected with RID2-specific antibodies (produced by our lab). The histone H3 antibody (Abcam, ab1791) and proteins detected by Ponceau S staining were used as the references.

### **Analysis of Antibiotic Resistance**

The seeds were placed directly on half-strength MS medium in the absence (Mock) and presence of 5  $\mu\text{g ml}^{-1}$  spectinomycin, 33  $\mu\text{g ml}^{-1}$  kanamycin, or 50  $\mu\text{g ml}^{-1}$  gentamicin. After 7 days, representative seedlings were photographed and chlorophyll content was analyzed as described by Porra et al. (Porra et al., 1989).

### **The Immunoblotting to Detect FIB1 and NOP56**

For detecting the protein levels of FIB1 and NOP56, total proteins were extracted with lysis buffer (50 mM Tris-HCl [pH 8.0], 10 mM EDTA, 1% SDS, 1 mM DTT, and protease inhibitors). The HSC70 protein levels was determined as a reference.

For gel filtration assays, seedlings (2 g) were ground thoroughly in lysis buffer (20 mM Tris-HCl [pH 7.5], 25 % glycerol, 20 mM KCl, 2 mM EDTA, 2.5 mM  $\text{MgCl}_2$ , 250 mM sucrose, 1 mM dithiothreitol, and protease inhibitors) at 4 °C. The resulting suspension was filtered through a mesh nylon filter (70  $\mu\text{m}$ ) and then centrifuged at 13,000 g for 20 min. Finally, the sample was filtered through a mesh nylon membrane (0.22  $\mu\text{m}$ ) and fractionated by gel filtration.

For protein immunoblots, the proteins were separated by SDS-PAGE and transferred to PVDF membranes. Immuno-detection was performed as described as previously (Wang et al., 2012). FIB1 and NOP56 antibodies were generated in our lab and the HSC70 antibody was purchased from Agrisera (AS09592).

### **Accession Numbers:**

Sequence data from this article can be found in the Arabidopsis Genome Initiative database under the following accession numbers: SMO2, At1g22270; ANAC082, At5G09330; RID2, AT2G17410; FIB, At5g52470; NOP56, At1g56110; HSC70, At5g02500.

### **SUPPLEMENTAL INFORMATION**

Supplemental information is available.

### **FUNDING**

This work was supported by the National Natural Science Foundation of China (32070208), the Outstanding Youth Foundation of Henan Province (No. 202300410041), the Programs for Team and Talents of Innovative Research (in Science and Technology) in Henan Province (No. 21IRTSTHN019 and 20HASTIT041), the Foundation of Henan Educational Committee (No. 212102110151) and the 111 Project (No. D16014) and the Guiding Funds of Central Government for Supporting the Development of the Local Science and Technology in Henan province (No. Z20221343006).

### **AUTHOR CONTRIBUTIONS**

Z.H. and Z.S. designed all experiments, analyzed the data and wrote the manuscript. Z.G., X.W., Y.L., A.X., C.W., Y.Z. A.B. and D.L. performed the experiments and prepared the data; Z.H., Z.S. and J.S.-V. edited and revised the manuscript.

### **CONFLICT OF INTERESTS**

The authors declare that they have no competing interests.

### **REFERENCES**

Barandun, J. , Hunziker, M. , and Klinge, S. (2018). Assembly and structure of the SSU

- processome—a nucleolar precursor of the small ribosomal subunit. *Curr Opin Struct Biol* **49**, 85–93.
- Black, J.J., Sardana, R., Elmir, E.W., and Johnson, A.W.** (2020). Bud23 promotes the final disassembly of the small subunit Processome in *Saccharomyces cerevisiae*. *PLoS Genetics* **16**, e1009215.
- Chen, P., Jäger, G., and Zheng, B.** (2010). Transfer RNA modifications and genes for modifying enzymes in *Arabidopsis thaliana*. *BMC Plant Biology* **10**, 1–19.
- Du, Y., An, W., Zhu, X., Sun, Q., Qi, J., and Ye, K.** (2020). Cryo-EM structure of 90S small ribosomal subunit precursors in transition states. *Science* **369**, 1477–1481.
- Farley-Barnes, K.I., Ogawa, L.M., and Baserga, S.J.** (2019). Ribosomopathies: old concepts, new controversies. *Trends in Genetics* **35**, 754–767.
- Figaro, S., Wacheul, L., Schillewaert, S., Graille, M., Huvelle, E., Mongeard, R., Zorbas, C., Lafontaine, D.L., and Heurgué-Hamard, V.** (2012). Trm112 is required for Bud23-mediated methylation of the 18S rRNA at position G1575. *Molecular and Cellular Biology* **32**, 2254–2267.
- Hang, R., Liu, C., Ahmad, A., Zhang, Y., Lu, F., and Cao, X.** (2014). Arabidopsis protein arginine methyltransferase 3 is required for ribosome biogenesis by affecting precursor ribosomal RNA processing. *Proceedings of the National Academy of Sciences* **111**, 16190–16195.
- Hang, R., Wang, Z., Yang, C., Luo, L., Mo, B., Chen, X., Sun, J., Liu, C., and Cao, X.** (2021). Protein arginine methyltransferase 3 fine-tunes the assembly/disassembly of pre-ribosomes to repress nucleolar stress by interacting with RPS2B in Arabidopsis. *Molecular Plant* **14**, 223–236.
- Heurgué-Hamard, V., Graille, M., Scrima, N., Ulryck, N., Champ, S., van Tilbeurgh, H., and Buckingham, R.H.** (2006). The zinc finger protein Ynr046w is plurifunctional and a component of the eRF1 methyltransferase in yeast. *Journal of Biological Chemistry* **281**, 36140–36148.
- Hu, Z., Cools, T., and De Veylder, L.** (2016). Mechanisms used by plants to cope with DNA damage. *Annual Review of Plant Biology* **67**, 439–462.

- Hu, Z., Qin, Z., Wang, M., Xu, C., Feng, G., Liu, J., Meng, Z., and Hu, Y. (2010). The Arabidopsis SM02, a homologue of yeast TRM112, modulates progression of cell division during organ growth. *The Plant Journal* **61**, 600–610.
- Kailasam, S., Singh, S., Liu, M.J., Lin, C.C., and Yeh, K.C. (2020). A HemK class glutamine -methyltransferase is involved in the termination of translation and essential for iron homeostasis in Arabidopsis. *New Phytologist* **226**, 1361–1374.
- Kanazawa, H., Saavedra, O.M., Maianti, J.P., Young, S.A., Izquierdo, L., Smith, T.K., Hanessian, S., and Kondo, J. (2018). Structure - Based Design of a Eukaryote - Selective Antiprotozoal Fluorinated Aminoglycoside. *Chem Med Chem* **13**, 1541–1548.
- Leihne, V., Kirpekar, F., Vågbø, C.B., Van den Born, E., Krokan, H.E., Grini, P.E., Meza, T.J., and Falnes, P.Ø. (2011). Roles of Trm9-and ALKBH8-like proteins in the formation of modified wobble uridines in Arabidopsis tRNA. *Nucleic Acids Research* **39**, 7688–7701.
- Li, W., Shi, Y., Zhang, T., Ye, J., and Ding, J. (2019). Structural insight into human N6amt1 - Trm112 complex functioning as a protein methyltransferase. *Cell Discovery* **5**, 1–13.
- Liu, Y., Deisenroth, C., and Zhang, Y. (2016). RP - MDM2 - p53 pathway: Linking ribosomal biogenesis and tumor surveillance. *Trends in Cancer* **2**, 191–204.
- Matos-Perdomo, E., and Machín, F. (2019). Nucleolar and ribosomal DNA structure under stress: yeast lessons for aging and cancer. *Cells* **8**, 779.
- Narla, A., and Ebert, B.L. (2010). Ribosomopathies: human disorders of ribosome dysfunction. *Blood, The Journal of the American Society of Hematology* **115**, 3196–3205.
- Ohbayashi, I., Konishi, M., Ebine, K., and Sugiyama, M. (2011). Genetic identification of Arabidopsis RID2 as an essential factor involved in pre - rRNA processing. *The Plant Journal* **67**, 49–60.
- Ohbayashi, I., Lin, C.-Y., Shinohara, N., Matsumura, Y., Machida, Y., Horiguchi, G., Tsukaya, H., and Sugiyama, M. (2017). Evidence for a role of ANAC082 as

- a ribosomal stress response mediator leading to growth defects and developmental alterations in Arabidopsis. *The Plant Cell* **29**, 2644–2660.
- Pasternak T, Tietz O, Rapp K, Begheldo M, Nitschke R, Ruperti B, Palme K. 2015.** Protocol: an improved and universal procedure for whole-mount immunolocalization in plants. *Plant Methods* **11**: 50.
- Porra, R., Thompson, W., and Kriedemann, P. (1989).** Determination of accurate extinction coefficients and simultaneous equations for assaying chlorophylls a and b extracted with four different solvents: verification of the concentration of chlorophyll standards by atomic absorption spectroscopy. *Biochimica et Biophysica Acta (BBA)-Bioenergetics* **975**, 384–394.
- Purushothaman, S.K., Bujnicki, J.M., Grosjean, H., and Lapeyre, B. (2005).** Trm11p and Trm112p are both required for the formation of 2-methylguanosine at position 10 in yeast tRNA. *Molecular and Cellular Biology* **25**, 4359–4370.
- Sáez-Vásquez, J., and Delseny, M. (2019).** Ribosome biogenesis in plants: from functional 45S ribosomal DNA organization to ribosome assembly factors. *The Plant Cell* **31**, 1945–1967.
- Sardana, R., and Johnson, A.W. (2012).** The methyltransferase adaptor protein Trm112 is involved in biogenesis of both ribosomal subunits. *Molecular Biology of the Cell* **23**, 4313–4322.
- Schnittger, A., and De Veylder, L. (2018).** The dual face of cyclin B1. *Trends in Plant Science* **23**, 475–478.
- Singh, S., Vanden Broeck, A., Miller, L., Chaker-Margot, M., and Klinge, S. (2021).** Nucleolar maturation of the human small subunit processome. *Science* **373**, eabj5338.
- Vanden Broeck, A., and Klinge, S. (2022).** An emerging mechanism for the maturation of the Small Subunit Processome. *Curr Opin Struct Biol* **73**, 102331.
- Van Tran, N., Ernst, F.G.M., Hawley, B.R., Zorbas, C., Ulryck, N., Hackert, P., Bohnsack, K.E., Bohnsack, M.T., Jaffrey, S.R., and Graille, M. (2019).** The human 18S rRNA m6A methyltransferase METTL5 is stabilized by TRMT112.

Nucleic Acids Research **47**, 7719–7733.

- Wang, W., Ryu, K.H., Bruex, A., Barron, C., and Schiefelbein, J.** (2020). Molecular basis for a cell fate switch in response to impaired ribosome biogenesis in the Arabidopsis root epidermis. *The Plant Cell* **32**, 2402–2423.
- Wang, Y., Carrie, C., Giraud, E., Elhafez, D., Narsai, R., Duncan, O., Whelan, J., and Murcha, M.W.** (2012). Dual location of the mitochondrial preprotein transporters B14. 7 and Tim23-2 in complex I and the TIM17: 23 complex in Arabidopsis links mitochondrial activity and biogenesis. *The Plant Cell* **24**, 2675–2695.
- Weis, B.L., Kovacevic, J., Missbach, S., and Schleiff, E.** (2015). Plant-specific features of ribosome biogenesis. *Trends in Plant Science* **20**, 729–740.
- Wu, S., Wang, Y., Wang, J., Li, X., Li, J., and Ye, K.** (2021). Profiling of RNA ribose methylation in Arabidopsis thaliana. *Nucleic Acids Research* **49**, 4104–4119.
- Yi, D., Alvim Kamei, C.L., Cools, T., Vanderauwera, S., Takahashi, N., Okushima, Y., Eekhout, T., Yoshiyama, K.O., Larkin, J., and Van den Daele, H.** (2014). The Arabidopsis SIAMESE-RELATED cyclin-dependent kinase inhibitors SMR5 and SMR7 regulate the DNA damage checkpoint in response to reactive oxygen species. *The Plant Cell* **26**, 296–309.
- Yoshiyama, K.** (2016) SOG1: a master regulator of the DNA damage response in plants. *Genes and Genetic Systems* **90**, 209–216.
- Zorbas, C., Nicolas, E., Wacheul, L., Huvelle, E., Heurgué-Hamard, V., and Lafontaine, D.L.** (2015). The human 18S rRNA base methyltransferases DIMT1L and WBSR22-TRMT112 but not rRNA modification are required for ribosome biogenesis. *Molecular Biology of the Cell* **26**, 2080–2095.

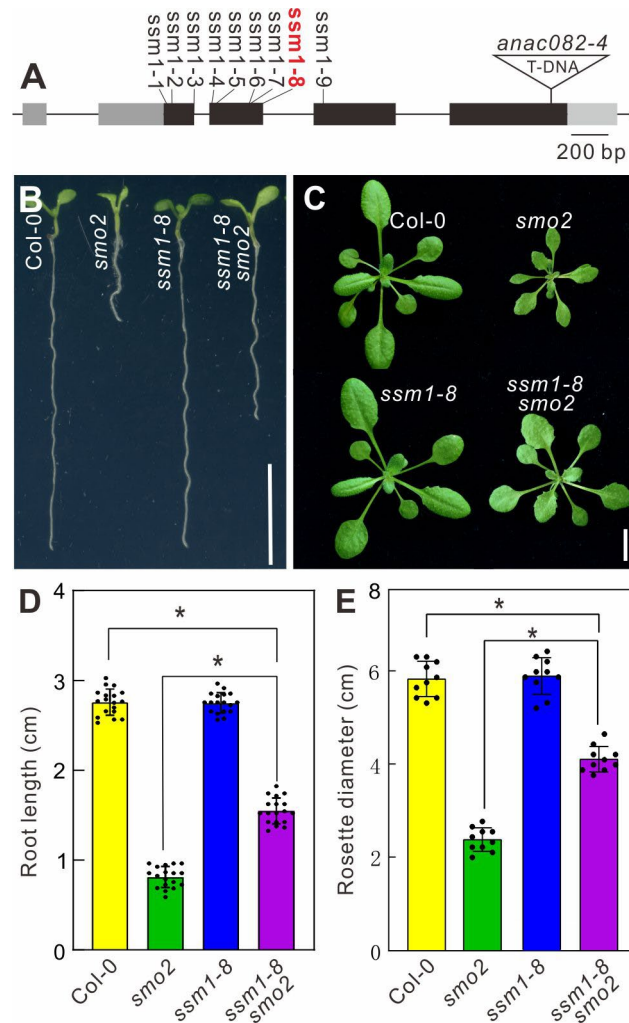


**Figure 1. The *ssm1* Mutation Restores Growth of the *smo2* Mutant.**

(A) Schematic representation of the *ANAC082* locus. The coding region of *ANAC082* (*AT5G09330*) is indicated as black rectangles and untranslated regions (UTRs) as gray rectangles. The T-DNA insertion in *anac082-4* is indicated by a triangle.

(B-C) Morphologies of 7-day-old seedlings (B) and 21-day-old plants (C) of Col-0, *smo2*, *ssm1-8*, and *ssm1-8 smo2*. Bars = 1 cm.

(D-E) Quantification of root length of 7-day-old seedlings (D) and rosette diameter of 21-day-old plants (E) of Col-0, *smo2*, *ssm1-8*, and *ssm1-8 smo2*. The widest diameter of rosette leaves from the leaf tips of opposite rosette leaves are measured. Data represent mean  $\pm$  SD ( $n > 18$ ). Statistically significant differences compared with wild-type (Col-0) plants are indicated; \*P value  $< 0.01$  (two-tailed Student's *t*-test).

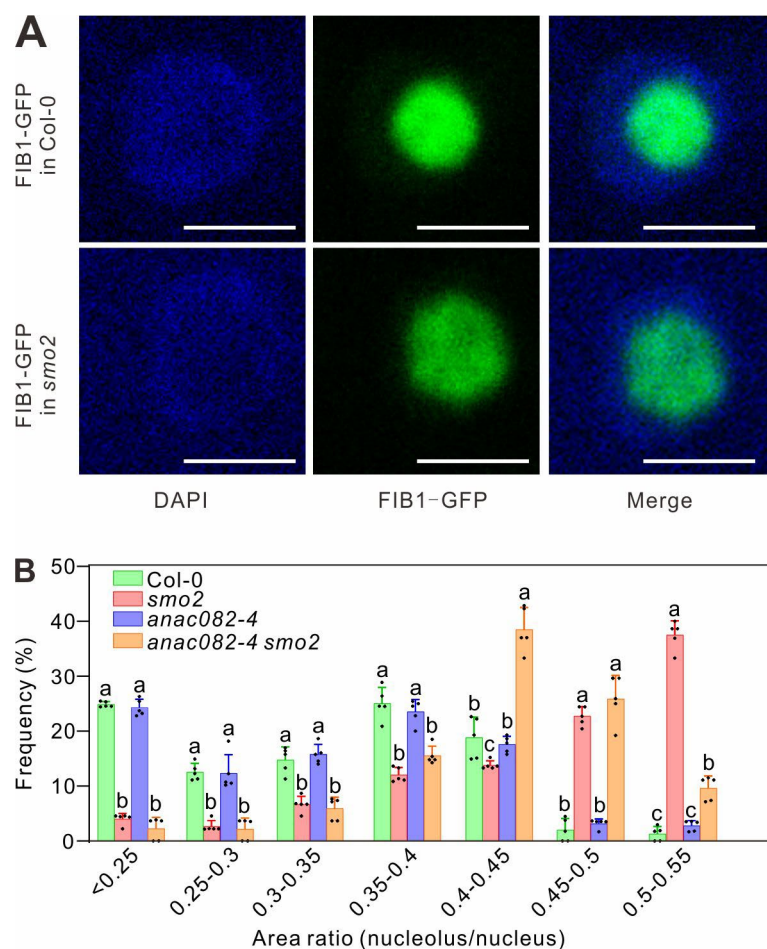


**Figure 2. The *smo2* Mutant Suffers from Nucleolar Stress.**

(A) The nucleolus is enlarged in the *smo2* mutant. Confocal laser-scanning micrographs of cells from the root elongation zone of 7-day-old seedlings of FIB1-GFP in Col-0 and FIB1-GFP in *smo2*. Nucleoli are marked by GFP and appear green, and the nuclei are stained with 4',6-diamidino-2-phenylindole (DAPI) and appear blue. Bars = 20  $\mu$ m.

(B) Quantification of area ratio (nucleolus/nucleus) of cells in root meristem zone of Col-0, *smo2*, *anac082-4*, and *anac082-4 smo2*. Five 7-d-old seedlings are analyzed for each genotype and more than 50 cells from each seedling are measured. The different letters indicate significant differences (ANOVA, Tukey's multiple comparisons test, P value < 0.05)

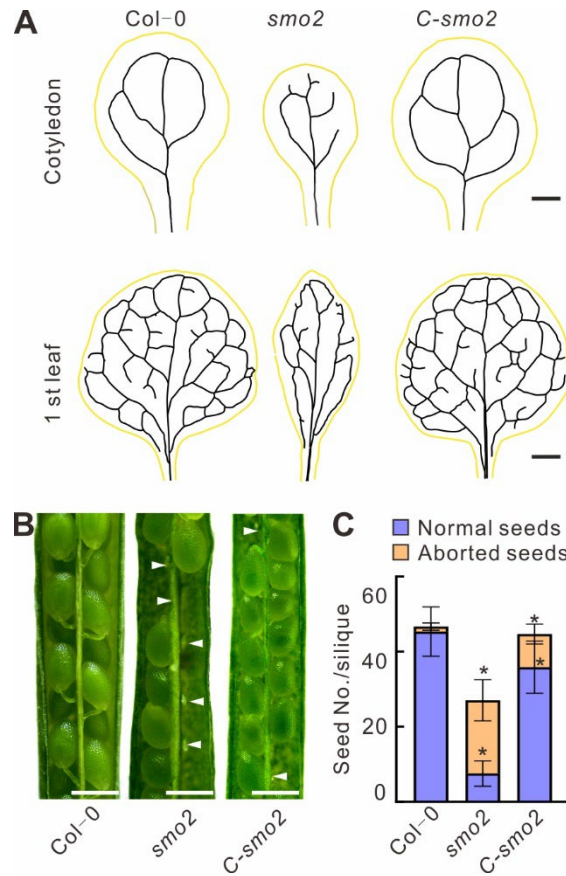


**Figure 3. The *smo2* Mutant Exhibits Developmental Defects in Venation and Seeds.**

**(A)** Venation patterns in the cotyledons (upper panel) and first-node leaves (bottom panel) from Col-0 (left), *smo2* (middle), and the *SMO2<sub>pro</sub>:SMO2* complementation line (*C-smo2*, right). The *smo2* mutant exhibits an aberrant pattern of veins in the cotyledon and a pointed shape in the first true leaf. Bars = 1 mm.

**(B)** Seeds in siliques from Col-0, *smo2*, and *C-smo2* at 16 days after pollination. The white arrows indicate the aborted ovules. Bars = 1 mm.

**(C)** Quantification of normal (blue) and aborted (yellow) seeds per silique of Col-0, *smo2*, and *C-smo2*. Data represent mean  $\pm$  SD ( $n > 15$ ). Statistically significant differences compared with wild-type (Col-0) plants are indicated; \*P value  $< 0.01$  (two-tailed Student's *t*-test).

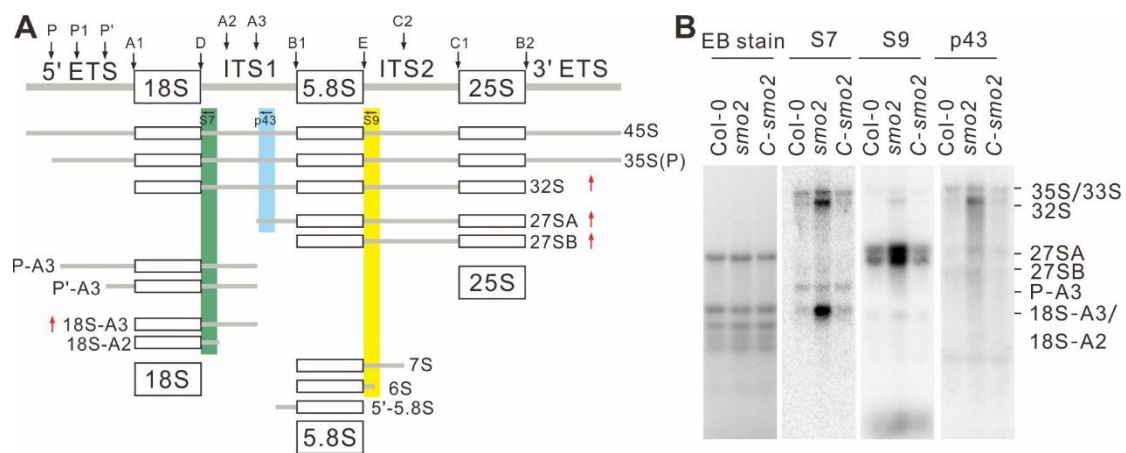


**Figure 4. Aberrant pre-rRNA Processing in the *smo2* Mutant.**

**(A)** Schematic diagram of various pre-rRNA processing intermediates. The pre-rRNA processing intermediates detected by northern blot analysis with specific probes are labeled with different colors and indicated by horizontal arrows. Black vertical arrows above the diagram indicate endonucleolytic cleavage sites. Red arrows indicate the rRNA intermediates that over-accumulated in the *smo2* mutant compared with Col-0. Scheme modified from Hang et al., (2013).

**(B)** The accumulation of pre-rRNAs in Col-0, *smo2*, and *C-smo2*. Northern blot analyses to detect the pre-rRNAs are performed using the probes (S7, S9, and p43) indicated in (A). The RNA is stained with ethidium bromide (EB stain) as a loading control.

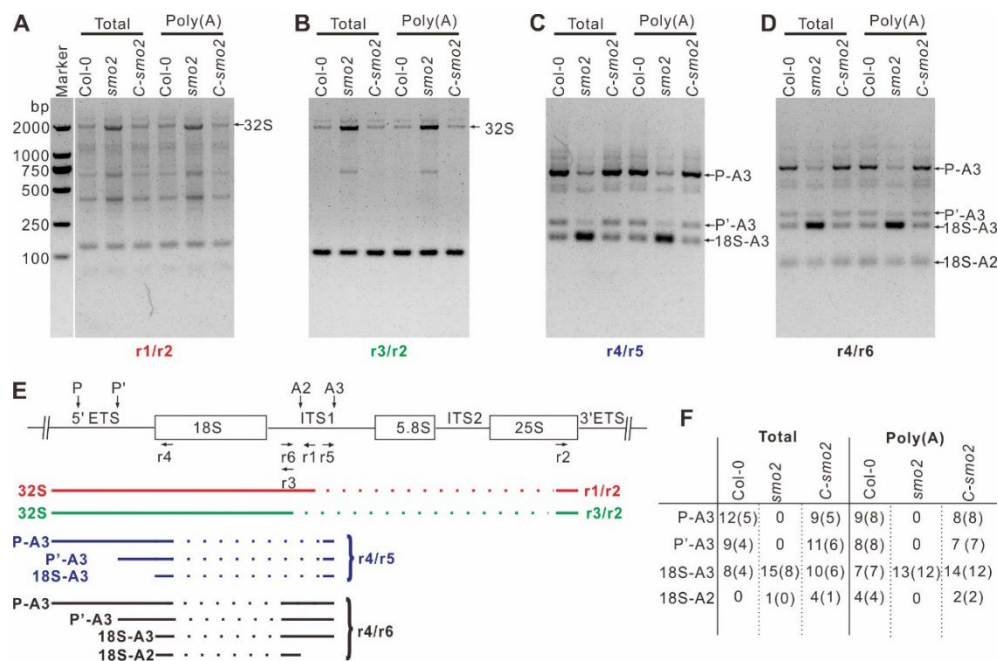


**Figure 5. Aberrant pre-rRNA Processing at the 3' and 5' Extremities in the *smo2* Mutant.**

(A-B) The accumulation of 32S intermediates amplified with the paired primers r1/r2 (A) and r3/r2 (B) in Col-0, *smo2*, and *C-smo2*.

(C-D) The accumulation of pre-18S rRNAs amplified using the paired primers r4/r5 (C) and r4/r6 (D) in Col-0, *smo2*, and *C-smo2*.

(E) Schematic diagram of the amplified PCR fragments. The positions of oligonucleotides r1–r6 used for PCR amplification of ligated 5' and 3' ends are indicated by horizontal arrows. The paired primers r1/r2 (A), r3/r2 (B), r4/r5 (C), and r4/r6 (D) indicated in (E) are used for the amplification of rRNA intermediates. Sizes of DNA markers (bp) are indicated on the left in (A).

(F) The results of cRT-PCR cloning of 18S intermediates (P-A3, P'-A3, 18S-A3, and 18S-A2). The cRT-PCR products used for cloning are derived from (D) using the r4/r6 primer pair. Poly(A), template reverse transcribed from oligo-dT purified RNA; Total, template reverse transcribed from total RNA. The number of clones obtained is indicated in the table, and the number of polyadenylated clones is marked in parentheses.

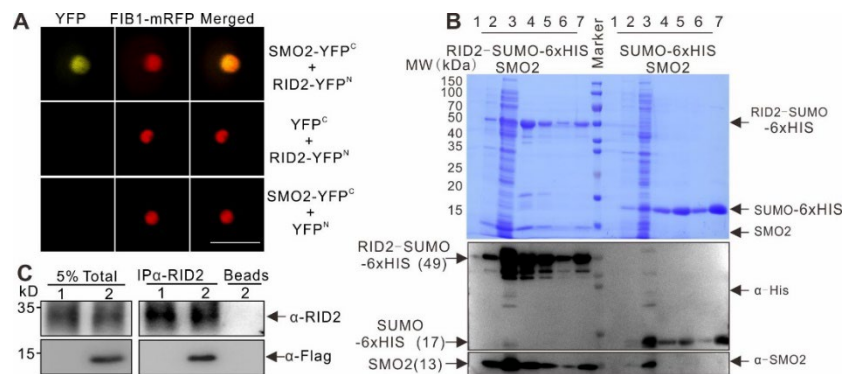


**Figure 6. SMO2 Interacts with RID2.**

**(A)** The BiFC assay in tobacco leaf cells. RID2 is fused to the N-terminal half of yellow fluorescent protein (RID2-YFP<sup>N</sup>) and SMO2 is fused to the C-terminal half of YFP (SMO2-YFP<sup>C</sup>). Reconstitution of YFP signal is observed in the nucleolus (upper panel), indicating a positive interaction, but no fluorescence is observed in the negative controls: YFP<sup>C</sup> (C-terminus of YFP alone) expressed with RID2-YFP<sup>N</sup> (middle panel) and YFP<sup>N</sup> (N-terminus of YFP alone) expressed with SMO2-YFP<sup>C</sup> (bottom panel). A plasmid expressing a nucleolar marker, FIB1-mRFP, is co-transformed with the plasmids indicated on the right. Bar = 20  $\mu$ m.

**(B)** The co-elution assay. RID2 is tagged at the C-terminus with SUMO-6xHIS (RID2-SUMO-6xHIS), and SUMO-6xHIS is used as negative control. RID2-SUMO-6xHIS and SUMO-6xHIS are co-expressed with untagged SMO2 (SMO2) in *E. coli* strain BL21 (DE3). Subsequently, the total protein is extracted for co-elution assays using a nickel affinity matrix. The resulting gels are stained with Coomassie blue (upper panel) or transferred to nitrocellulose for the detection of RID2 with His antibody (anti-His, middle panel) and SMO2 with SMO2-specific antibody (anti-SMO2, bottom panel). Different samples from the cells co-expressing RID2-SUMO-6xHIS with SMO2 (left) and those co-expressing SUMO-6xHIS with SMO2 (right) are separated on an SDS-PAGE gel and labeled as follows: uninduced culture (1), induced total bacterial extract (2), flow-through (3), co-elution in a 50 mM imidazole-containing buffer (15  $\mu$ L of eluted fraction in each lane, 4, 5, and 6); co-elution in a 100 mM imidazole-containing buffer (15  $\mu$ L of eluted fraction, 7), and molecular mass marker (8). Molecular weight (MW) is shown in kDa on the left.

**(C)** The co-immunoprecipitation assay. Total protein from 7-d-old seedling of Col-0 and 35S:SMO2-Flag plants is extracted for the co-immunoprecipitation and specific antibody against RID2 is used for detecting RID2 protein and commercial Flag antibody is for SMO2.

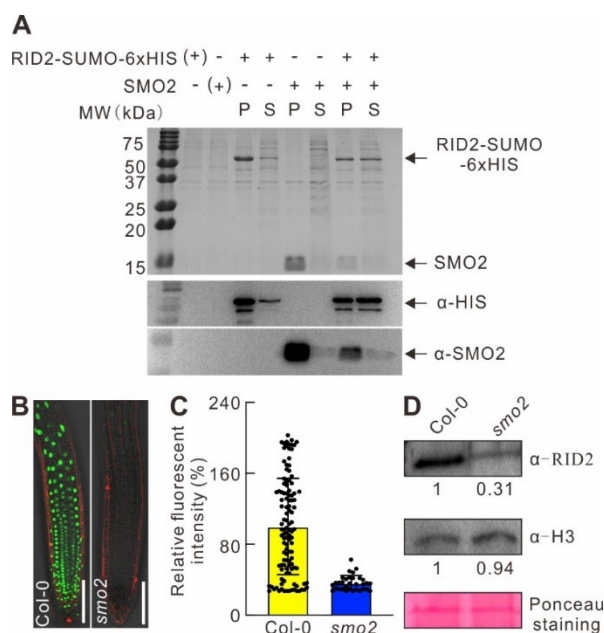


**Figure 7. SMO2 Controls RID2 Stability.**

**(A)** The solubility of RID2 in *E. coli* cells. RID2-SUMO-6xHIS and SMO2 are expressed in *E. coli* strain BL21 (DE3), either separately or together, with compatible plasmids. The first two lines indicate the presence (+) and absence (-) of plasmids expressing the indicated proteins. Except for the non-induced control cultures, all cell extracts are centrifuged to separate inclusion bodies (P) and soluble proteins (S), as indicated on the third line. The proteins are separated by electrophoresis in a 15% SDS-PAGE gel and are stained with Coomassie blue. MW kDa: Molecular mass standards. A similar gel is subjected to western blotting to detect RID2-SUMO-6xHIS with anti-His antibody (anti-His, middle panel) and SMO2 with a SMO2-specific antibody (anti-SMO2, bottom panel).

**(B)** Representative images of fluorescence in *RID2-GFP/Col-0* (Left panel) and *RID2-GFP/smo2*. A transgenic plant harboring a single-copy of the  $35S_{pro}:RID2-GFP$  construct (*RID2-GFP/Col-0*) is crossed with the *smo2* mutant to generate a  $35S_{pro}:RID2-GFP$  plant in the *smo2* background (*RID2-GFP/smo2*). Bars = 100  $\mu$ m.

**(C)** Quantification of fluorescent intensity per cell in the *smo2* mutant relative to Col-0 plants. Data represent mean  $\pm$  SD ( $n > 30$ ). Statistically significant differences compared with wild-type (Col-0) plants are indicated; \*P value  $< 0.01$  (two-tailed Student's *t*-test).

**(D)** RID2 level in Col-0 and the *smo2* mutant. The total protein is extracted for the detection of RID2 with a RID2-specific antibody ( $\alpha$ -RID2) and histone H3 with a commercial antibody ( $\alpha$ -H3, the reference). The blot is stained with Ponceau S as a loading control. Value of RID2 or histone H3 in Col-0 is set as 1; the number below *smo2* indicates the relative abundance of RID2 or histone H3.

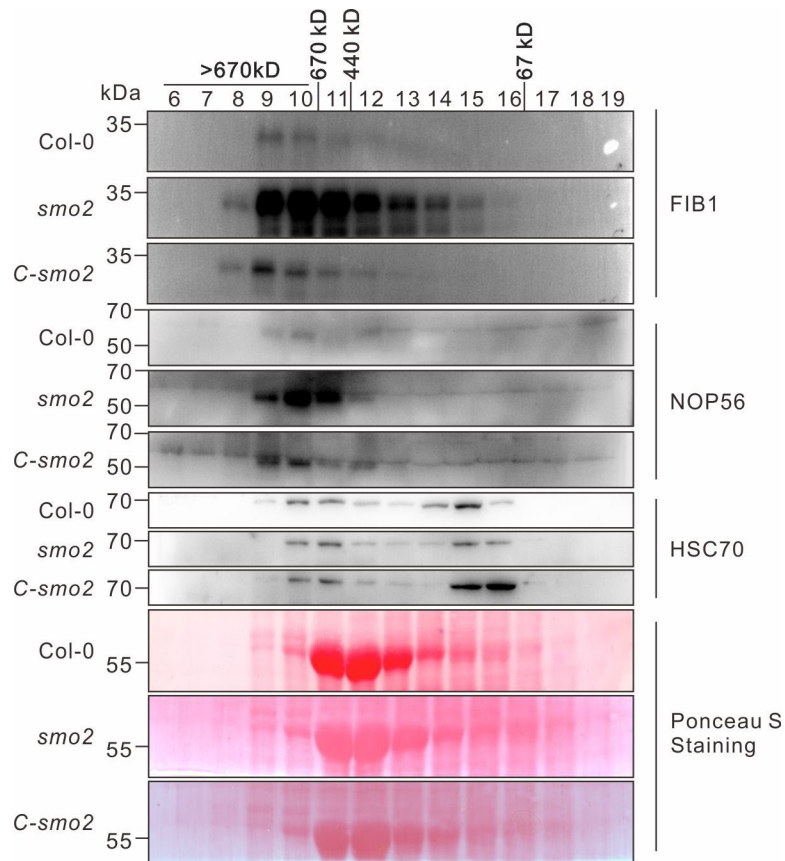


**Figure 8. FIB1 and NOP56 Accumulated in the Larger Complex of the SSU Processome in the *smo2* Mutant.**

Gel-filtration patterns of FIB1 and NOP56 in wild type (Col-0), *smo2*, and *C-smo2*. Total protein lysates are extracted and separated by gel filtration. The resulting fractions are loaded onto 12% SDS-PAGE gels. FIB1 and NOP56 are detected by western blotting with specific antibodies. HSC70 is detected with a commercial antibody and the membranes stained with Ponceau S are used as the reference.

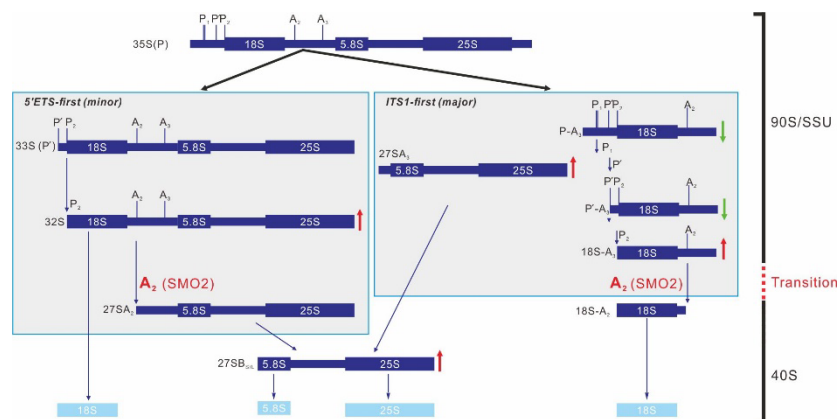


**Figure 9. The Roles for SMO2 in 45S Pre-rRNA Processing.**

SMO2 is proposed to specifically participate in the A<sub>2</sub> cleavage of pre-rRNAs. SMO2 deficiency reduces the cleavage efficiency at the A<sub>2</sub> site, which results in the over-accumulation of 32S and 18S-A<sub>3</sub>. As the processing of pre-rRNAs from 35S pre-rRNA to mature rRNAs (18S, 25S, 5.8S) is a sequential process, a defect at the A<sub>2</sub> cleavage step may delay the transition of the 90S Processome to the pre-40S, which may reduce subsequent cleavages, as indicated by the over-accumulation of 27SA/27SB. The accumulated 90S/SSU Processome may accelerate cleavages at the P' and P<sub>2</sub> sites, as indicated by the reduction of the levels of P'-A<sub>3</sub> and P-A<sub>3</sub>. Red arrows indicate over-accumulated pre-rRNAs (↑) and green arrows indicate depleted pre-rRNAs (↓) in the *smo2* mutant, as detected by RNA gel blots and circular RT-PCR assays. Scheme modifies from Saez-Vasquez and Delseny (2019).